Asia-Pac. J. Atmos. Sci., 50(2), 229-237, 2014
DOI:10.1007/s13143-014-0011-z

The Role of ENSO in Global Ocean Temperature Changes during 1955-2011 Simulated with a 1D Climate Model

Roy W. Spencer and William D. Braswell

Earth System Science Center, University of Alabama in Huntsville, Alabama, U. S. A.

(Manuscript received 26 April 2013; accepted 21 August 2013)

Abstract: Global average ocean temperature variations to 2,000 m depth during 1955-2011 are simulated with a 40 layer 1D forcing-feedback-mixing model for three forcing cases. The first case uses standard anthropogenic and volcanic external radiative forcings. The second adds non-radiative internal forcing (ocean mixing changes initiated in the top 200 m) proportional to the Multivariate ENSO Index (MEI) to represent an internal mode of natural variability. The third case further adds ENSO-related radiative forcing proportional to MEI as a possible natural cloud forcing mechanism associated with atmospheric circulation changes. The model adjustable parameters are net radiative feedback, effective diffusivities, and internal radiative (e.g., cloud) and non-radiative (ocean mixing) forcing coefficients at adjustable time lags. Model output is compared to Levitus ocean temperature changes in 50 m layers during 1955-2011 to 700 m depth, and to lag regression coefficients between satellite radiative flux variations and sea surface temperature between 2000 and 2010. A net feedback parameter of 1.7 W m^{-2} K^{-1} with only anthropogenic and volcanic forcings increases to 2.8 W m^{-2} K^{-1} when all ENSO forcings (which are one-third radiative) are included, along with better agreement between model and observations. The results suggest ENSO can influence multi-decadal temperature trends, and that internal radiative forcing of the climate system affects the diagnosis of feedbacks. Also, the relatively small differences in model ocean warming associated with the three cases suggests that the observed levels of ocean warming since the 1950s is not a very strong constraint on our estimates of climate sensitivity.

Key words: Climate sensitivity, climate change, climate modeling, ENSO, ocean heat content

1. Background and justification

Climate modeling in the context of global warming research is usually performed with coupled atmosphere-ocean general circulation models (AOGCMs) which simulate the time evolving nature of the 3D climate system based upon a combination of physical first principles and approximations, e.g., the Coupled Model Intercomparison Project (CMIP3; CMIP5) models (Meehl *et al*., 2007; Taylor *et al*., 2012). While 3D modeling may be the ultimate methodology, current models still have limitations.

Corresponding Author: Roy W. Spencer, UAH Earth System Science Center, 320 Sparkman Drive, Huntsville, Alabama 35805, U. S. A.
E-mail: roy.spencer@nsstc.uah.edu

For example, the 20th Century and SRESa1b simulations from the CMIP3 coupled climate models reveal a wide range of ocean temperature trends during 1955-2010, the period during which ocean temperature profile observations are available for comparison. Of thirteen models we examined (Fig. 1), three models experienced net ocean heat loss, despite imposed positive radiative forcing (Forster and Taylor, 2006) which should have caused a net warming of the model ocean. This suggests the possibility of energy conservation issues in the CMIP3 models (Gupta *et al*., 2012), although small energy imbalances at model initialization could also result in this behavior. Since anthropogenic global warming is caused by small energy imbalances (changes in the radiative energy balance of the Earth causing changes in total heat content of the ocean), this presents a problem. It should be noted that Lindzen (2002) used a simple model and found that changes in ocean heat content were not a good constraint on climate sensitivity.

Furthermore, the potential role of natural modes of climate variability in multi-decadal temperature change is still not well understood. For example, the El Niño (warm) phase of the El Niño - Southern Oscillation (ENSO, Rasmussen and Carpenter, 1982) was more intense than the La Niña phase for about 30 years starting in the late 1970s (Wolter, 1987; Jin *et al*., 2003), a behavior which AOGCMs cannot yet explain. This is shown in Fig. 2, a plot of the Multivariate ENSO Index (MEI, Wolter, 1987) which is positive during El Niño conditions, and negative during La Niña conditions. Here we will use MEI rather than the NINO-3 or NINO-3.4 indices due to it representing the larger-scale manifestation of ENSO activity. While one theory claims that anthropogenic global warming has caused El Niño activity to become more frequent or more intense than La Niña activity (Trenberth and Hoar, 1995), it is also possible that there is a natural, low frequency modulation of El Niño and La Niña activity, as evidenced by persistent or unusually strong El Niño conditions experienced approximately during 1920 to 1940 (see Fig. 2), which is arguably before human greenhouse gas emissions could have reasonably been blamed. Such natural variability can complicate our identification and understanding of anthropogenic forcing of the climate system (e.g., Tsonis *et al*., 2007), a point further evidenced by less than expected surface warming since the late 1990s.

For example, if the atmospheric circulation changes associ-

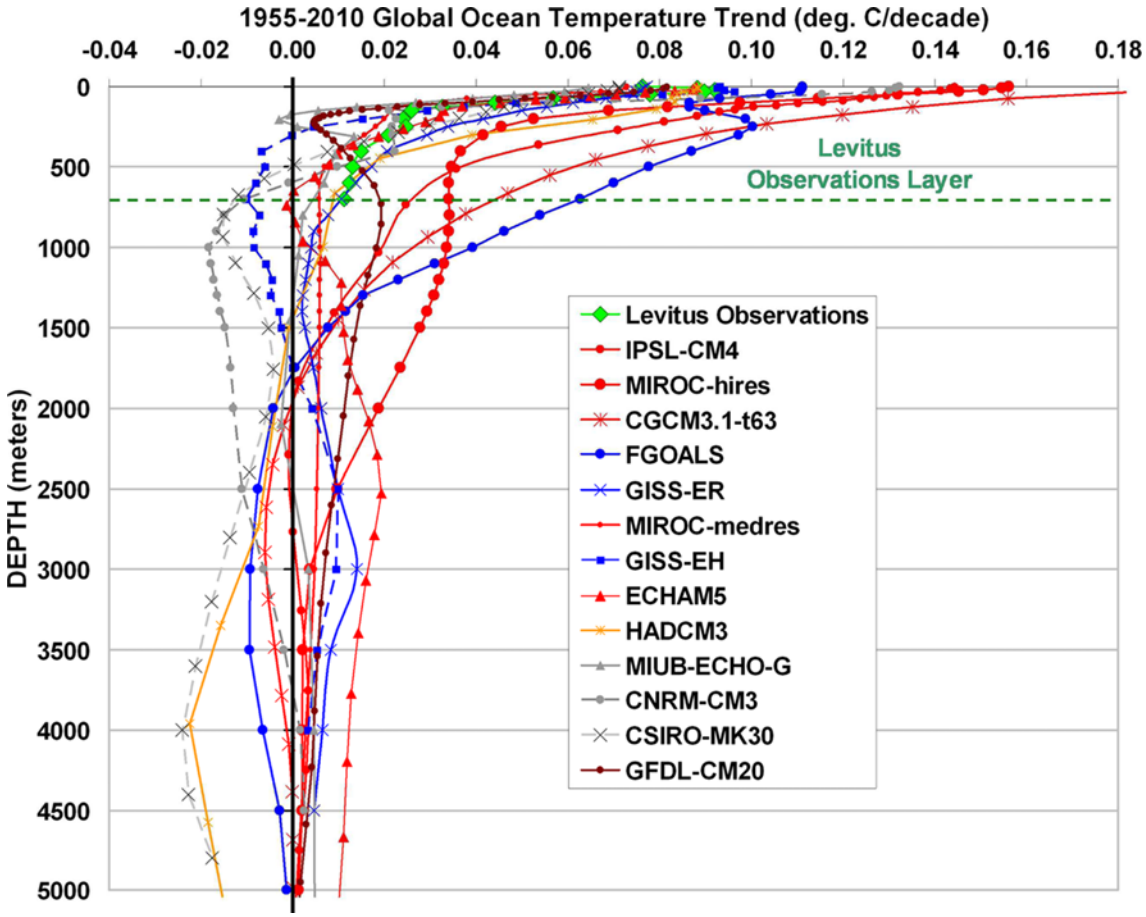

Fig. 1. Ocean temperature trends over the period 1955 through 2010 as a function of depth for the global oceans (+/– 60° latitude) calculated from observations (Levitus) and 13 CMIP3 coupled climate models.

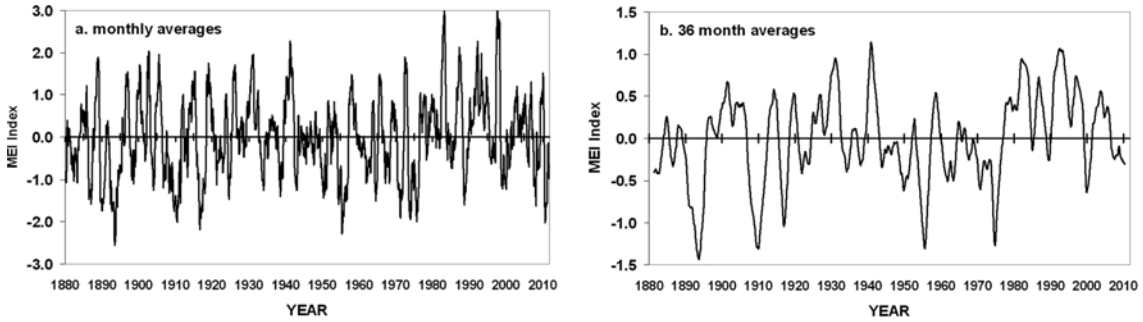

Fig. 2. Multivariate ENSO Index between 1880 and 2011 at (a) monthly and (b) 36 month time resolution. The original MEI data extends from 1950 to the present, while pre-1950 data are reconstructed based upon less extensive data.

ated with more frequent El Niño activity cause a slight change in global average cloud cover - a change which is not merely a feedback upon surface temperature -- the resulting "internal" radiative forcing of the climate system (Spencer and Braswell, 2010) could confound our diagnosis of how sensitive the system is to "external" radiative forcing from anthropogenic greenhouse gases and aerosols. Even if this does not occur, the changes in oceanic overturning during El Niño and La Niña can cause decadal time scale surface warming and cooling which complicate the identification of anthropogenic temperature trends (e.g., Solomon and Newman, 2012).

Since explaining recent increases in the heat content of the ocean represent extremely small energy imbalances on the order of 1 part in 1,000 (e.g., Levitus *et al*., 2012), it seems reasonable to use a simplified model where energy balance can simply be assumed at the outset. For global averages, transient changes in surface or ocean mixed layer temperature anomalies (departures from the average annual cycle) are dominated by only three processes: (1) radiative forcing, (2) net radiative feedback, and (3) ocean mixing. These three processes can be

modeled, albeit simply, in a single (vertical) dimension. While the detailed physics giving rise to complex climate system behaviors such as ENSO would be difficult to create in a 1D model, the vertical redistribution of thermal energy in response to the known history of ENSO events can be used as a pseudo-forcing of the model. If we ignore land-ocean exchanges of energy, the total heat content of the ocean is independent of horizontal transports associated with ENSO; there is only a net change in vertical mixing, and associated changes in feedback losses of energy at the top of the ocean.

We can then use the MEI index to explore the extent to which internal non-radiative forcing (ENSO-related changes in the ocean temperature profile) versus internal radiative forcing (non-feedback changes in ENSO-related radiative balance) contribute to explaining a variety of observations between 1955 and 2011. The novel aspect of the approach is establishing evidence for the postulated existence of ENSO-related atmospheric circulation changes associated with ENSO which change the global ocean radiative budget independent of average surface temperature changes. Importantly, evidence for ENSO-related radiative forcing of temperature would involve the atmospheric radiative changes preceding the ocean temperature changes, after internal ocean mixing changes have already been accounted for. These atmospheric changes could involve some combination of cloud shortwave albedo, cloud longwave, or water vapor changes.

Here we will use a 1D forcing-feedback-mixing model to help explain natural modes of climate variability superimposed upon a general warming trend assumed to be mostly anthropogenic in origin. The model is simpler than previous 1D ocean models (e.g., Harvey & Hwang, 2001, and references therein) because (1) it only addresses departures from the average state, with no annual cycle; and (2) net vertical transports of heat are accomplished only through depth-dependent effective diffusivities (κ_v) operating on vertical gradients of temperature departures from the mean state. Regarding the first simplification, an annual cycle is unnecessary for the task at hand since there is no physical reason to suspect that multi-decadal global warming is caused by the seasons; also, the seasonal phase-locked nature of El Niño and La Niña (which peak during Northern Hemisphere winter) can be imposed upon the model from the observed history of ENSO activity.

Similarly, the second simplification assumes that there is an average oceanic temperature profile, including a thermocline, which the ocean relaxes to when there are temperature perturbations away from that profile. This relaxation is accomplished with an "effective diffusivity" which represents all processes responsible for vertical redistribution of heat anomalies in the ocean, including the thermohaline circulation and turbulent ocean mixing of all types which act to restore the system to its average state. It is recognized that diffusion does not generally act as a restoring mechanism, and ocean transport is not always down-gradient. The primary intent is to include a simple mechanism to allow heating of the surface to mix downward, as expected with anthropogenic global warming. A range of depth-dependent effective diffusivities are swept to find a set which provides a good match between the resulting model simulation and the variety of observations. The effective diffusivities do not vary with time; we believe the inclusion of such variability would be intractable computationally.

The primary question we will address is: What combination of assumed climate sensitivity (net feedback parameter), ocean effective diffusivities, and ENSO-related pseudo-forcings best describe the depth-dependent ocean temperature changes during 1955-2011? An important additional test of model behavior is the lag regression relationship between global average sea surface temperature (SST) from HadSST2 (Rayner *et al*., 2006) and top-of-atmosphere radiative flux variations since 2000 as measured by CERES (Clouds and the Earth's Radiant Energy System, Wielicki *et al*., 1996). As will be shown, this lag behavior is important from the standpoint of determining the extent to which radiative flux variations are a combination of (1) radiative feedback upon temperature (which would be nearly simultaneous with temperature change) versus (2) radiative forcing of temperature (which would precede temperature change). This issue regarding the direction of causation between variations in temperature and radiative flux was explored in some detail by Spencer and Braswell (2010, 2011), as well as Lindzen and Choi (2011).

2. Observed ocean temperature variations 1955-2011

Global (+/–60^o latitude) three-monthly ocean temperature variations from Levitus *et al.* (2009) for the period JFM 1955 through AMJ 2011 were averaged into 50 m layers to a depth of 700 m and interpolated to monthly time resolution. The results in Fig. 3a for the top four layers, the bottom layer, and the 0-700 m average show general warming which decreases with depth.

The strong interannual variability in Fig. 3a is mostly related to ENSO activity. It is well known that ENSO is the dominant mode of interannual variability in the climate system, and we see from Fig. 3b that the warm phase of ENSO (El Niño) leads to a reduction in the rate of vertical overturning of the global average ocean, evidenced by warming in the 0 to 100 m layer, and cooling below. Our intent is not to explain why this occurs, only to exploit the observed relationship for the purposes of the 1D model.

While it is difficult for a simple 1D model to include the physics causing ENSO (even some 3D coupled climate models have difficulty), it is relatively easy to include the ENSO-induced vertical heat redistribution and the resulting changes in radiative feedback at the top of the ocean. For the purpose of forcing ENSO variability upon the model, we use the Multivariate ENSO index from 1950 to 2011, and the extended MEI for the period 1880-1950 (Wolter and Timlin, 2011) during the model spin-up. The MEI is a quantitative empirical measure of the intensity of El Niño (positive MEI) and La Niña (negative MEI) conditions, computed as the first unrotated principal component of six observed variables over the tropical

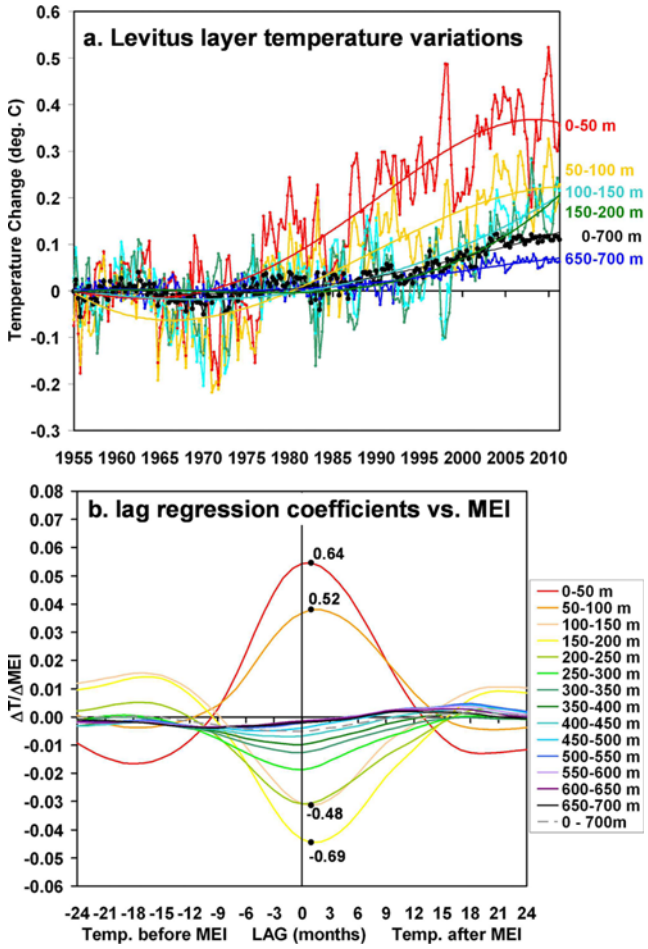

Fig. 3. Three-monthly Levitus global (+/–60° latitude) ocean temperature variations from JFM 1955 through AMJ 2011 averaged into 50 m layers: (a) 0-50 m, 50-100 m, 100-150 m, 150-200 m, 650-700 m, and 0-700 m; and (b) detrended layer temperatures lag regressed against the Multivariate ENSO Index, with lag = +1 correlation coefficients shown for the top four layers. The +/−1σ confidence intervals approximately equals the width of the four data point dots.

Pacific: sea-level pressure, zonal and meridional components of the surface wind, sea surface temperature, surface air temperature, and total fractional coverage of the sky by clouds. The MEI is normalized to have a standard deviation of 1.

The basis for our simplified partitioning of ocean mixing changes associated with ENSO come from the MEI and ocean temperature data themselves. Lag regression coefficients between the global average ocean layer temperatures and MEI during 1955-2011 (Fig. 3b) reveal warming of the 0-100 m layer, and cooling of the 100-200 m layer, during El Niño conditions (positive MEI), and the opposite behavior during La Niña (negative MEI). This global-average behavior provides the basis for representing the ENSO-induced changes in ocean mixing with exchanges in heat between the 0-100 m layer and the 100-200 m layer in the 1D model.

Initially it will be assumed that ENSO-related temperature changes are only the result of these changes in ocean mixing between the warm near-surface layers above the thermocline (0-100 m) and the colder layers below, as modified by changes in feedback which are (by definition) proportional to surface temperature departures from normal. It will be included in the time-dependent 1D forcing-feedback-mixing model to explore the relative roles of forcing and feedback in explaining the ocean temperature changes during 1955-2011, as well as the satellite-observed variations in top-of-atmosphere (TOA) net radiative flux variations between 2000 and 2010. It will be shown that internal radiative forcing associated with ENSO, possibly the result of changes in cloud cover, is additionally required in order to explain the satellite TOA radiative flux variations, which cannot be explained based upon ocean mixing and feedback alone.

3. The forcing-feedback-mixing model

The simple 1D model used here will include the three primary processes that control global average surface (or ocean mixed layer) temperature departures from equilibrium: forcing, feedback, and ocean vertical mixing. We address monthly and longer time scales so that we can assume the atmosphere is in convective equilibrium with the ocean surface; potential changes in latent and sensible heat transfer from the ocean to the atmosphere are neglected, except to the extent they are implied by the feedback parameter, which implicitly includes all atmospheric changes in response to surface temperature change.

The model is represented in schematic form in Fig. 4, with solid arrows representing radiative energy exchanges, and dashed arrows representing non-radiative energy exchanges. The ocean-only model of temperature departures from equilibrium uses forty 50 m-thick layers extending from the ocean surface to 2,000 m depth. Energy exchanges between land and ocean are neglected. The radiative influence and response of the atmosphere is implicitly included in the model's feedback and radiative forcing parameters. The model equations for the time rate of change of temperature in each of the 40 layers are:

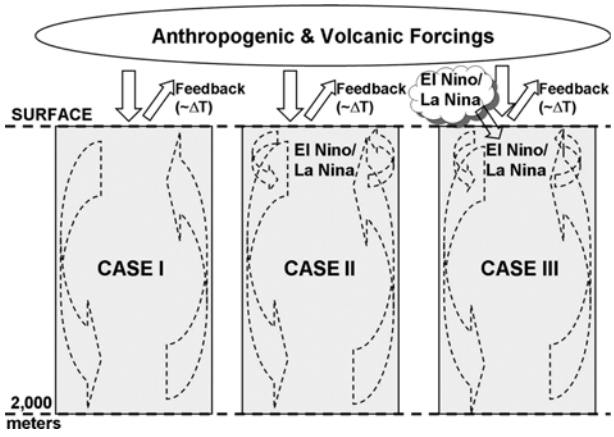

Fig. 4. Schematic representation of the 1D forcing-feedback-mixing model. Solid arrows represent radiative energy exchanges, while dashed arrows represent non-radiative energy exchanges.

$$C_p[d\Delta T_1/dt] = [N(t) - \lambda\Delta T_1] + S_1(t) + C_p\kappa_{v1}d^2\Delta T/dz^2, \quad (1)$$

$$C_p[d\Delta T_2/dt] = S_2(t) + C_p\kappa_{v2}d^2\Delta T/dz^2, \quad (2)$$

$$C_p[d\Delta T_3/dt] = S_3(t) + C_p\kappa_{v3}d^2\Delta T/dz^2, \quad (3)$$

$$C_p[d\Delta T_4/dt] = S_4(t) + C_p\kappa_{v4}d^2\Delta T/dz^2, \quad (4)$$

$$C_p[d\Delta T_i/dt] = C_p\kappa_{vi}d^2\Delta T/dz^2 \ (i = 5,40) \quad (5)$$

where Cp is the bulk heat capacity of a 50 m thick ocean layer, assumed to be a constant with depth; N represents all external and internal radiative forcings; λ is the net feedback parameter (Forster and Taylor, 2006; Forster and Gregory, 2006); S represents non-radiative forcing of temperature change (ocean mixing), with N and S in Watts per sq. meter (W m^{-2}); and the last term represents all processes which mix vertical temperature anomaly structures with depth, with κ_v being the depth-dependent effective diffusivity representing all vertical mixing processes in the global-average ocean. Note the left hand side of Eqs. 1-4 is equivalent to the change in the layer heat content with time. The two terms in brackets together in Eq. 1 represent the total radiative imbalance of the system: the sum of radiative forcing and radiative feedback.

We assume the total radiative forcing N operating on the first model layer is composed of the RCP6 anthropogenic and volcanic external forcings estimated by Meinshausen *et al.* (2011) used in the CMIP5 experiments, with land use and black carbon forcing removed for our ocean-only simulations, and an internal pseudo-forcing proportional to MEI with empirically determined coefficient of proportionality α at adjustable time lag j:

$$N(t) = N_{RCP}(t) + \alpha*\mathrm{MEI}(t_j). \quad (6)$$

The non-radiative forcing terms of the first four model layers (S) represent inter-layer heat exchange components proportional to MEI with empirically determined coefficient of proportionality β at adjustable time lag k:

$$S_1(t) = 0.5\beta*\mathrm{MEI}(t_k), \quad (7)$$

$$S_2(t) = 0.5\beta*\mathrm{MEI}(t_k), \quad (8)$$

$$S_3(t) = -0.5\beta*\mathrm{MEI}(t_k), \quad (9)$$

$$S_4(t) = -0.5\beta*\mathrm{MEI}(t_k). \quad (10)$$

The MEI terms in Eqs. 7-10 are meant to approximate the observed relationship between upper ocean temperature variations and MEI shown in Fig. 3b by imposing ENSO vertical heat exchanges associated with El Niño and La Niña activity; for example, warming of the 0-100 m layer and an equal amount of cooling in the 100-200 m layer during El Niño (positive MEI) conditions. While this obviously forces considerable agreement between the model and the observations on interannual time scales, the model ocean must still respond in terms of vertical mixing and radiative feedback, which then alters the total heat content of the model climate system and the deeper ocean temperature profile.

The ten adjustable free parameters of the model are the net feedback parameter; scale factors on the radiative and non-radiative MEI forcings; time lags on the radiative MEI forcing; and six depth dependent effective diffusivities. Ranges of all model adjustable parameters are swept over many thousands of combinations, each resulting in a model simulation which is then compared to the observations.

4. Model simulations with and without ENSO

All experiments are run with the CMIP5 RCP6 radiative forcing histories (Meinshausen *et al.*, 2011), but different assumed combinations of MEI-dependent forcings, net feedback parameter, and ocean effective diffusivities. For simplicity, the ocean diffusivities are assumed to be constant with time, and adjustable for only the top six layers, with the remainder of the layers assumed to have the same diffusivity as the sixth (250-300 m) layer. The ranges of the free parameters tested were 0.5 to 4.0 W m^{-2} K^{-1} for the net feedback parameter; 0 to 4.7×10^{-4} m^2 s^{-1} for the diffusivities; and +/– 12 months lag (relative to the observed time history of MEI) for the ENSO radiative forcings.

The experiments involve initialization of the model in the first month of 1880 with zero temperature anomalies (equilibrium) and are run with a monthly (30.438 day) time step through June 2011. Initialization of the model at the start of the Levitus observational period (1955) rather than in 1880 was found to only reinforce our conclusions. The model output was then compared to the Levitus observations for the period 1955-2011, and to the CERES satellite observations of net radiative flux variations during March 2000 through December 2010.

Various combinations of the model free parameters were tested in a heuristic fashion, by sweeping a range for each adjustable parameter as described above. The model results quickly suggested much narrower ranges of the free parameters over which the model behaved in a manner similar to the observations. The free parameter values that produced good agreement with the observations were chosen in an iterative fashion as the dependence of the model results on the various free parameters was better understood. This tuning of the simple 1D model parameters is little different philosophically from the tuning of various parameterizations performed in 3D models, except in the case of the feedback parameter which we adjust directly whereas it is adjusted indirectly in 3D models as other parameters (such as cloud parameterizations) upon which it depends are adjusted.

Three forcing experiments were run, as shown schematically in Fig. 4. Case I includes only the RCP6 estimates of anthropogenic and volcanic radiative forcings to ensure that the feedback parameter (i.e., climate sensitivity) results were consis-

Table 1. Model free parameter values chosen for optimized fit to observations under different simulation forcing scenarios, and the resulting fraction of 0-2000 m layer heating occurring below 700 m depth.

Parameter	Case I: RCP6 only	Case II: RCP6 + ENSO mixing	Case III: RCP6 + ENSO mixing + ENSO radiative
Feedback parameter (λ, W m^{-2} K^{-1})	1.7	1.9	2.8
MEI non-radiative forcing coeff. (α, W m^{-2})	N.A.	1.2	1.2
α time lag (months)	N.A.	Assumed +1	Assumed +1
MEI radiative forcing coeff. (β, W m^{-2})	N.A.	N.A.	0.6
β time lag (months)	N.A.	N.A.	–9
Layers 1-6 effective diffusivities (κ, 10^{-4} m^2 s^{-1})	0.54, 0.84, 1.1, 1.8, 3.0, 4.7	0.74, 1.3, 2.6, 3.6, 4.2, 4.7	0.72, 1.2, 2.4, 4.2, 4.7, 4.7
Fraction of 0-2000 m heating occurring below 700 m depth	0.40	0.44	0.39

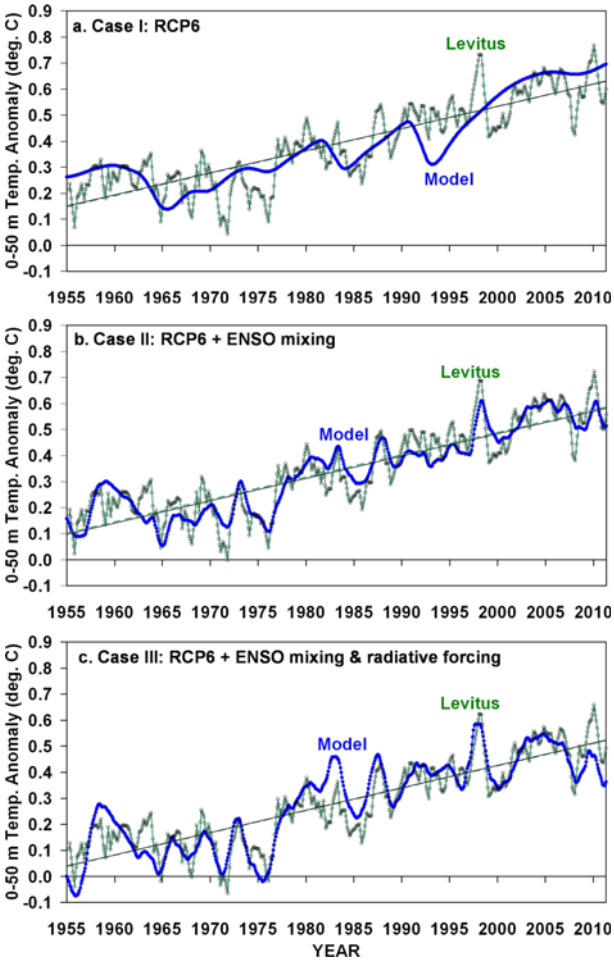

Fig. 5. Model simulations of monthly global average 0-50 m layer ocean temperature variations for three cases: (a) only RCP6 radiative forcings; (b) RCP6 plus ENSO-related non-radiative forcing (ocean mixing); and (c) RCP6 plus ENSO-related radiative and non-radiative forcings.

tent with the CMIP3 models (Forster and Taylor, 2006). Case II adds to the RCP6 forcings ENSO non-radiative forcing (ocean mixing) based upon the time history of the MEI index, with a time lag of 1 month to be consistent with the Levitus observations in Fig. 3b. Case III further adds ENSO-related radiative forcing with adjustable time lag.

Example values of the free parameters which were deemed to provide good overall agreement to the observations for the three cases are given in Table 1, keeping in mind that other slightly different values produced nearly the same results. In all three cases, the model was required to match the 0-50 m observed temperature trend for 1955-2011 to within 0.002 deg. C per decade. None of the time series were detrended for the purpose of the comparisons, since temperature trends are one component of the observations we want to explain.

The 0-50 m model temperature results for the three simulation case scenarios are shown in Fig. 5. All of the model linear trends for the 1955-2011 equal the Levitus trend, while the free parameters were adjusted to optimize the match between the model and the other observations. In Case I, the warming is only the result of the increasing anthropogenic greenhouse gas forcing in RCP6, while the intermittent cooling events are from major volcanic eruptions. The Case I feedback parameter is $\lambda = 1.7$ W m^{-2} K^{-1} (climate sensitivity of 2.2°C, assuming 3.7 W m^{-2} forcing from a doubling of atmospheric carbon dioxide, 2 × CO2) which is within the range of diagnosed net feedback parameters from IPCC (2007) AR4 coupled climate models ($\lambda = 0.9$ to 1.9 W m^{-2} K^{-1}, Forster and Taylor, 2006). This suggests the simple model produces a net feedback parameter consistent with CMIP models in response to anthropogenic and volcanic forcings.

In Case II, the impact of the imposed ENSO-related heat exchanges is evident, showing much better agreement with observations (Fig. 5b) for year-to-year variability as would be expected since the model is being nudged in that direction at each time step based upon the time history of ENSO through the MEI index. The feedback parameter in this simulation is $\lambda = 1.9$ W m^{-2} K^{-1}, which corresponds to a slightly lower climate sensitivity of 2.0°C.

Finally, adding the internal radiative forcing from ENSO in Case III (Fig. 5c) leads to only small adjustments to the model 0-50 m layer temperatures, but a rather large increase in the feedback parameter, $\lambda = 2.8$ W m^{-2} K^{-1}, corresponding to a climate sensitivity of 1.3°C. The reason for this change will become apparent shortly.

The temperature trend profiles for the three model cases are shown in Fig. 6. The Levitus trend profile shape is better matched when the effects of ENSO are included, although the

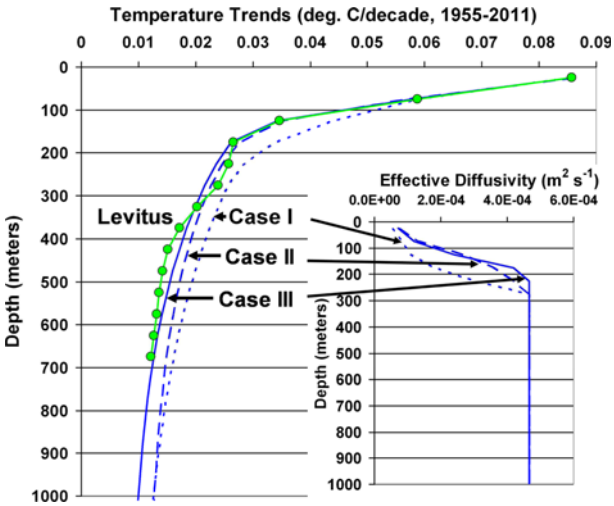

Fig. 6. Comparison of three model cases to observed decadal ocean temperature trends as a function of depth, in 50 m layers, for 1955-2011. The layer effective diffusivities used in the model simulations are shown in the inset.

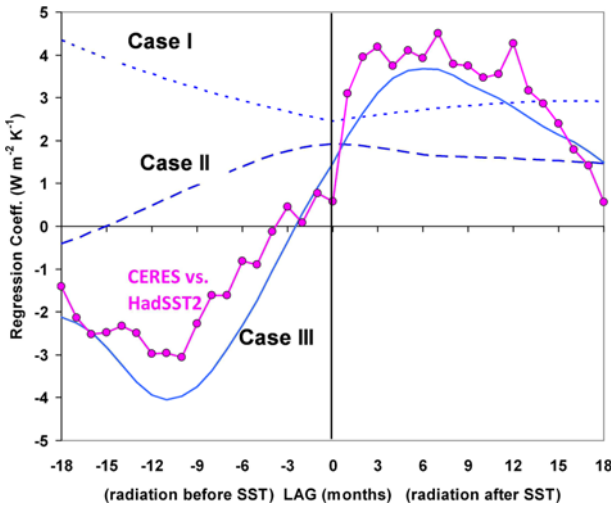

Fig. 7. Lag regression coefficients between monthly CERES radiative fluxes and HadSST2 sea surface temperature variations, and compared to the three model simulations.

differences between the three simulation cases are within the margin of error of the Levitus observations. In all three model cases, the fraction of the 0-2000 m layer warming occurring below 700 m depth (Case I:0.402; Case II:0.440; Case III: 0.389) is consistent with the one-third factor estimate obtained from observations (Levitus *et al*., 2012), given the margin of observational error.

But the largest differences between the model simulations and observations is found for the relationship between TOA radiative fluxes and SST during the period which the Terra satellite CERES instrument was operating (SST departures in the model are assumed to be the same as the 0-50 m layer temperature departures). The CERES Terra Satellite SSF 2.6 monthly global gridpoint radiative flux anomalies were averaged over the 60°N-60°S oceans for direct comparison to the Levitus and HadSST2 ocean surface temperatures. Significantly, the lag regression relationship between radiative flux and surface temperature (Fig. 7) can reasonably match the CERES vs. SST observations only if ENSO-related radiative forcing is included in the model. In Case II, where the only radiative effect is feedback upon the ENSO mixing-forced ocean temperature variations, the model is unable to capture the radiant energy accumulation (loss) which precedes the highest (lowest) temperature anomaly conditions.

In Case III, the greatest agreement with observations was found when the assumed ENSO radiative forcing (with its assumed proportionality constant, see Eq. 6) preceded the MEI index by around nine months. This is a significant result. It suggests that as part of the changes in the coupled ocean-atmosphere circulation associated with ENSO, there are non-feedback changes in the global radiative balance which occur that contribute to later surface temperature anomalies associated with ENSO, possibly through changes in cloud cover and the resulting global albedo. Feedback upon previous ENSO activity cannot explain the lag, as evidenced by the Case II curve in Fig. 7.

The most obvious (but not necessarily correct) explanation for this behavior is that the Earth's radiative budget is a partial function of circulation regime associated with El Niño and La Niña activity, independent of radiative feedback upon temperature. From Table 1 we see that the estimated magnitude of this internal radiative forcing is 0.6 W m^{-2} per unit MEI index. Compared to the estimate a rate of energy absorption/loss by the climate system of 240 W m^{-2}, this amounts to a 0.25% non-feedback modulation of the average global radiative energy budget by ENSO activity. Thus, the extended period of El Niño activity starting in the late 1970s appears to impact our interpretation of the sensitivity of the climate system to anthropogenic forcing by providing additional radiative heating of the climate system, which then implies a lower climate sensitivity in order to explain the same amount of temperature rise, at both the surface and within the ocean.

The model results also address the issue of the relative size of radiative forcing versus radiative feedback associated with ENSO (Dessler, 2011). Even though the non-radiative (ocean mixing) forcing in Case III was twice the size of the radiative forcing (see Table 1), supporting the Dessler (2011) view that ENSO is a primarily ocean-driven phenomenon, that smaller radiative forcing is still 2.8 times larger than the radiative feedback, with monthly standard deviations of 0.51 W m^{-2} and 0.18 W m^{-2} respectively over the ten-year satellite observation period. This is because radiative feedback is, by definition, proportional to surface temperature changes, which are very small in the global average. This supports the contention of Spencer and Braswell (2010) that short term internal radiative forcing can corrupt our estimates of radiative feedback in the climate system.

Finally, note that the common practice of diagnosing the feedback parameter at zero time lag would lead to a 50%

underestimate of the specified feedback for Case III in Fig. 7 (1.4 diagnosed vs. 2.8 W m^{-2} K^{-1} specified), consistent with the conclusions of Spencer and Braswell (2010, 2011) and Lindzen and Choi (2011) that the presence of time varying radiative forcing tends to lead to an underestimate of the net feedback parameter diagnosed from observations.

5. Conclusions

While it is easy to criticize the simplicity of a 1D model of the climate system, for global averages there are only three main processes which control surface (or ocean mixed layer) temperatures: radiative forcing, radiative feedback, and vertical ocean mixing, all of which can be included in a 1D model. Given the wide variety of ocean responses in the more complex 3D models (see Fig. 1), it is entirely reasonable to use a simple 1D model which can include these three main processes in an attempt to best explain observed rates of ocean warming. Insights gained through such a simple model can then help guide the development and tuning of the much more complex 3D models.

The 1D forcing-feedback-mixing model results presented here suggest that radiative changes generated within the climate system associated with ENSO can have a considerable impact on our interpretation of ocean temperature changes and our inferences regarding feedback. Forcing of the model with only the traditional external forcings (mainly anthropogenic and volcanic) and adjusting the model ocean effective diffusivities to match the observed warming profiles down to 700 m since 1955 yields a climate sensitivity within the range of the CMIP3 climate models.

Adding ENSO non-radiative forcing (imposed exchanges of heat between the 0-100 m and 100-200 m layers proportional to the Multivariate ENSO Index) did not substantially change the optimum net feedback parameter, but the resulting radiative behavior of the model could not capture the satellite-observed time-lag relationship between radiative flux and temperature. Only with the inclusion of ENSO related radiative forcing nine months prior to peak MEI (El Niño or La Niña conditions) could the lag relationship between satellite measured global oceanic radiative flux variations during 2000 through 2010 be reasonably well reproduced, which in turn required a substantially larger net feedback parameter in the model, 50% larger than with anthropogenic and volcanic forcings alone. This is interpreted as evidence that stronger El Niño activity, such as that experienced approximately between 1977 and 2006, causes internal radiative forcing of the climate system, which supplements anthropogenic warming.

Nevertheless, the relatively small differences in the ocean warming profile for the three modeled cases in Fig. 6 - despite a 50% range in assumed climate sensitivity - suggest that the levels of ocean warming observed since the 1950s might not provide a very strong constraint on our estimates of climate sensitivity. The uncertainty in the rates of ocean mixing and the exceedingly small changes in deep ocean temperature contribute to this difficulty in diagnosing the sensitivity of the climate system.

Acknowledgments. We acknowledge the modeling groups, the Program for Climate Model Diagnosis and Intercomparison (PCMDI) and the WCRP's Working Group on Coupled Modeling (WGCM) for their roles in making available the WCRP CMIP3 multi-model dataset; support of this dataset is provided by the Office of Science, U.S. Department of Energy. This research was supported by NOAA contract NA07OAR4170503 and DOE contract DE-FG02-04ER63841.

Edited by: Song-You Hong, Kim and Yeh

REFERENCES

Dessler, A. E., 2011: Cloud variations and the Earth's energy budget. *Geophys. Res. Lett.,* **38**, L19701, doi:10.1029/2011GL049236.

Forster, P. M., and J. M. Gregory, 2006: The climate sensitivity and its components diagnosed from Earth Radiation Budget data. *J. Climate,* **19**, 39-52.

_____, and K. E. Taylor, 2006: Climate forcings and climate sensitivities diagnosed from coupled climate model integrations. *J. Climate,* **19**, 6181-6194.

Gupta, Alexander Sen, Les C. Muir, Jaclyn N. Brown, Steven J. Phipps, Paul J. Durack, Didier Monselesan, and Susan E. Wijffels, 2012: Climate drift in the CMIP3 models. *J. Climate,* **25**, 4621-4640.

Harvey, L. D., and Z. Huang, 2001: A quasi-one-dimensional coupled climate-change cycle model 1. Description and behavior of the climate component. *J. Geophys. Res.,* **106**, 22,339-22,353, doi:10.1029/2000-JC000364.

Intergovernmental Panel on Climate Change (IPCC), 2007: *Climate Change 2007: The Physical* Science Basis. Contribution of Working Group I to the Fourth Assessment Report of the *Intergovernmental Panel on Climate Change*, edited by S. Solomon et al., Cambridge Univ. Press, New York, 996 pp.

Jin, F.-F., S. I. An, A. Timmermann, and J. Zhao, 2003: Strong El Niño events and nonlinear dynamical heating. *Geophys. Res. Lett*., **30(3)**, 1120, doi:10:1029/2002GL016356.

Levitus, S., J. I. Antonov, T. P. Boyer, R. A. Locarnini, H. E. Garcia, and A. V. Mishonov, 2009: Global ocean heat content 1955-2008 in light of recently revealed instrumentation Problems. *Geophys. Res. Lett.,* **36**, L07608, doi:10. 1029/2008GL037155.

_____, and Coauthors, 2012: World ocean heat content and thermosteric sea level change (0-2000 m), 1955-2010. *Geophys. Res. Lett.,* **39**, L10603, doi:10.1029/2012GL051106.

Lindzen, R. S., 2002: Do deep ocean temperature records verify models? *Geophys. Res. Lett*., **29**, 10.1029/2001GL014360 .

_____, and Y.-S. Choi, 2011: On the observational determination of climate sensitivity and its implications. *Asia-Pac. J. Atmos. Sci*., **47**, 377-390, doi:10.1007/s13143-011-0023-x.

Meehl, G. A., C. Covey, T. Delworth, M. Latif, B. McAvaney, J. F. B. Mitchell, R. J. Stouffer, and K. E. Taylor, 2007: The WCRP CMIP3 multiÅ]model data set: A new era in climate change research. *Bull. Amer. Meteor. Soc.,* **88**, 1383-1394.

Meinshausen, M., and Coauthors, 2011: The RCP Greenhouse Gas Concentrations and their Extension from 1765 to 2300. *Climatic Change*, doi:10.1007/s10584-011-0156-z.

Rasmussen, E. M., and T. H. Carpenter, 1982: Variations in tropical sea surface temperature and surface wind fields associated with the Southern Oscillation/El Niño. *Mon. Wea. Rev.,* **110**, 354-384.

Rayner, N. A., P. Brohan, D. E. Parker, C. K. Folland, J. J. Kennedy, M. Vanicek, T. Ansell, and S. F. B. Tett, 2006: Improved analyses of changes and uncertainties in sea surface temperature measured in situ since the mid-nineteenth century: the HadSST2 data set. *J. Climate,* **19**, 446-469.

Solomon, A., and M. Newman, 2012: Reconciling disparate 20th century Indo-Pacific ocean temperature trends in the instrumental record. *Nature Climate Change*, **2**, 691-699, doi:10.1038/nclimate1591.

Spencer, R. W., and W. D. Braswell, 2010: On the diagnosis of radiative feedback in the presence of unknown radiative forcing. *J. Geophys. Res.,* **115**, doi:10.1029/2009JD013371.

_____, and _____, 2011: On the misdiagnosis of surface temperature feedbacks from variations in Earth's radiant energy balance. *Remote Sens.,* **3**, 1603-1613, doi:10.3390/rs3081603.

Taylor, K. E., R. J. Stouffer, and G. A. Meehl, 2012: An overview of CMIP5 and the experiment design. *Bull. Amer. Meteor. Soc*., **93**, 485-498.

Trenberth, K., and T. J. Hoar, 1995: The 1990-1995 El Niño-Southern Oscillation event: Longest on record. *Geophys. Res. Lett*., **23**, 57-60.

Tsonis, A. A., K. Swanson, and S. Kravtsov, 2007: A new dynamical mechanism for major climate shifts. *Geophys. Res. Lett*., **34**, L13705, doi:10.1029/2007GL030288.

Wielicki, B. A., B. R. Barkstrom, E. F. Harrison, R. B. Lee III, G. L. Smith, and J. E. Cooper, 1996: Clouds and the Earth's Radiant Energy System (CERES): An Earth Observing System experiment. *Bull. Amer. Meteor. Soc.,* **77**, 853-868.

Wolter, K., 1987: The Southern Oscillation in surface circulation and climate over the tropical Atlantic, Eastern Pacific, and Indian Oceans as captured by cluster analysis. *J. Climate Appl. Meteor.,* **26**, 540-558.

_____, and M. S. Timlin, 2011: El Niño/Southern Oscillation behaviour since 1871 as diagnosed in an extended multivariate ENSO index (MEI.ext). *Int. J. Climatol*., **31**, 1074-1087, doi:10.1002/joc.2336.